Mesoscopic phase separation dynamics of compressible copolymer melts

N. M. Maurits, B. A. C. van Vlimmeren, and J. G. E. M. Fraaije
Groningen Biomolecular Sciences and Biotechnology Institute, Bioson Research Institute, Department of Biophysical Chemistry, University of Groningen, Nijenborgh 4, 9747 AG Groningen, The Netherlands
(Received 31 October 1996)

In this paper we extend the dynamic mean-field density functional method, derived from the generalized time-dependent Ginzburg-Landau theory, to the mesoscopic dynamics of *compressible* polymer liquids. We discuss and compare different classes of compressibility models: exactly incompressible, the Helfand's harmonic penalty model, and a cell model. We present numerical results and show that the penalty model is a very practical and easy to use solution. In the current nVT ensemble dynamics algorithms application of the cell model leads to a variation of the pressure and, depending on conditions, the system develops liquid-gas transitions. We show that the morphology of a phase separated diblock copolymer melt around a gas bubble has intruiging structures, with lamellar phases oriented towards the gas-liquid interface. [S1063-651X(97)12707-6]

PACS number(s): 61.25.Hq, 64.60.My, 64.30.+t, 64.70.Ja

I. INTRODUCTION

A. General

The dynamic mean-field density functional model provides a numerical method for the simulation of coarse-grained morphology dynamics in polymer liquids [1]. The theory is a modification of model B [2,3], i.e., a generalized time-dependent Ginzburg-Landau theory for conserved order parameter.

In [2–7] and references cited therein, one can find numerous examples of computer simulations of time-dependent Ginzburg-Landau models for two-component incompressible liquids with linear transport coefficients and fourth-order phenomenological expansion models for the free energy. In general, the goal of mesoscopic polymer modeling is to obtain a theory of coarse-grained ordering phenomena in polymer liquids, based on a molecular description. We use a free energy functional, derived for a collection of Gaussian chains in a mean-field environment. In this approach we try to retain as much as possible of the underlying molecular detail, i.e., the architecture and composition of the chain molecules are important parameters. To this end, we do not use an expansion of the free energy in the order parameters, as is commonly done in Ginzburg-Landau models, but rather we use a single chain inverse density functional description for intrinsic chemical potentials. Previously, we studied the random term [8], the Gaussian chain density functional [9], and the relation with fourth-order expansions [10]. Some results of numerical calculations of phase separation in *incompressible* block copolymer melts and concentrated surfactant solutions were discussed in [1] and [11], respectively. Further studies of kinetic coefficients and the relation with microscopic force-field models are in progress.

In this paper our main objective is to consider *existing* models for the compressibility of polymer liquids and especially their application in the mesoscopic dynamics algorithms. We discuss three models: exactly incompressible, Helfand's harmonic penalty model, and a cell model. In the homogeneous equilibrium limit we find an equation of state similar, but not identical, to the Flory-Orwoll-Vrij (FOV) theory [12].

B. Equations of state for polymer liquids and their application to dynamic density functional theory

A large number of equations of state are based on lattice models [13]. The Simha-Somcynski theory [14–16] can be represented in terms of reduced pVT parameters, which is convenient for parameter selection [17,18]. The lattice-fluid model of Sanchez and Lacombe and modifications thereoff [19–21] accurately predict liquid-vapor transitions but they do not seem suited for the liquid state [22,23]. A big disadvantage of all lattice models is that they severely underestimate the pressure [24].

The FOV equation of state [12,25–27] is a cell model, fundamentally of the van der Waals type, in which the cohesive interactions are independent of the excluded volume interactions. It is widely used in polymer applications [23,28]. Since the most frequently used equations of state for polymer liquids seem to be derived either from the FOV cell model or lattice models, we propose to use a slightly modified FOV cell model for the numerical calculation of morphology dynamics in this paper.

A different class of models is based on integral equation approaches [29]. In the future the polymer reference interaction site model [30–32] may offer an accurate *ab initio* calculation of compressibility effects in polymer liquids. However, integral equation theories have inherent serious inconsistencies in the pressure calculations [29]. The numerical aspects are also cumbersome: solving the complex integral equations together with our dynamic equations does not seem possible at present. In contrast, the simple modified FOV compressibility model that we propose here is not computationally intensive and describes the most important physical excluded volume effects reasonably accurate.

Finally, in the polymer engineering world a number of empirical equations of state are also used [33,34], e.g., that of Spencer and Gilmore (an adapted van der Waals model) [35] and the Tait equation (see, e.g., [22] and [34]). Empiri-

cal equations of state often yield very good approximations of experimental pVT data [22]. The disadvantage of empirical equations is, of course, that it is difficult to predict the parameters from physical models. The parameters involved in the cell model and Helfand's penalty function can be derived from experimental data which make the models very well fit for numerical calculations.

We will show that in numerical applications it is sometimes more convenient to use a penalty function for high densities than the proposed cell model. The penalty function combines the effects of cohesive interactions (which favor clustering) and excluded volume interactions (which favor homogeneity). A harmonic penalty for density fluctuations about the mean bulk density was used by Helfand [36] and later by many others (e.g., [37]).

The paper is organized as follows. We briefly recall the dynamic mean-field density functional method and discuss the connection with the cell model and Helfand's harmonic penalty function. We show how the various models affect the microphase separation dynamics and, in addition, present results of numerical calculations of microphase separation in a compressible diblock copolymer melt, using the penalty and cell model. We compare the results with those obtained from an earlier simulation of phase separation dynamics in an incompressible system with similar composition.

II. THEORY

A. General

We shortly repeat the main part of the theory of the mesoscopic dynamics algorithms. For more details see [1]. For simplicity, we focus here on binary diblock copolymer melts; extensions to multicomponent copolymer mixtures are trivial. We consider a melt of volume V, containing n Gaussian chains, each of length $N=N_A+N_B$. There are two concentration fields $\rho_A(\mathbf{r})$ and $\rho_B(\mathbf{r})$, two external potentials $U_A(\mathbf{r})$ and $U_B(\mathbf{r})$, and two intrinsic chemical potentials $\mu_A(\mathbf{r})$ and $\mu_B(\mathbf{r})$.

Imagine that on a course-grained time scale, there is a certain collective concentration field $\rho_I(\mathbf{r})$ of the beads of type I (A or B). A bead is a statistical unit consisting of a fluctuating string of (usually 5 to 15) monomers [38,39]. Given this concentration field a free energy functional $F[\rho]$ can be defined as follows:

$$\beta F[\rho]=-n\ \ln\Phi+\ln n!-\beta\sum_I\ \int U_I(\mathbf{r})\rho_I(\mathbf{r})d\mathbf{r}+\beta F^{\rm nid}[\rho]. \tag{1}$$

Here Φ is the partition functional for the ideal Gaussian chains in the external field U_I, and $F^{\rm nid}[\rho]$ is the contribution from the nonideal interactions. The free energy functional is derived from an optimization criterium [1] which introduces the external potential as a Lagrange multiplier field. The external potentials and the concentration fields are related via a density functional for ideal Gaussian chains

$$\rho_I[U](\mathbf{r})=n\sum_{s'=1}^{N}\delta^K_{Is'}{\rm Tr}_c\psi\delta(\mathbf{r}-\mathbf{R}_{s'}). \tag{2}$$

Here $\delta^K_{Is'}$ is a Kronecker δ function with value 1 if bead s' is of type I and 0 otherwise. The trace ${\rm Tr}_c$ is limited to the integration over the coordinates of one chain

$${\rm Tr}_c(\cdot)=\mathcal{N}\int_{V^N}(\cdot)\prod_{s=1}^{N}d\mathbf{R}_s,$$

$\mathcal{N}$ is a normalization constant. ψ is the single chain configuration distribution function

$$\psi=\frac{1}{\Phi}\,e^{-\beta[H^G+\Sigma_{s=1}^{N}U_s(\mathbf{R}_s)]}, \tag{3}$$

where H^G is the Gaussian chain Hamiltonian

$$\beta H^G=\frac{3}{2a^2}\sum_{s=2}^{N}(\mathbf{R}_s-\mathbf{R}_{s-1})^2, \tag{4}$$

with a the Gaussian bond length parameter. The density functional is bijective; for every set of fields $\{U_I\}$ there is exactly one set of fields $\{\rho_I\}$. Thus there exists a *unique* inverse density functional $U_I[\rho]$. There is no known closed analytical expression for the inverse density functional, but for our purpose it is sufficient that the inverse functional can be calculated efficiently by numerical procedures.

We split the nonideal free energy functional formally into two parts

$$F^{\rm nid}[\rho]=F^c[\rho]+F^e[\rho],$$

where F^e contains the excluded volume interactions and F^c the cohesive interactions. The intrinsic chemical potentials μ_I are defined by the functional derivatives of the free energy

$$\mu_I(\mathbf{r})\equiv\frac{\delta F}{\delta\rho_I(\mathbf{r})}=-U_I(\mathbf{r})+\frac{\delta F^c}{\delta\rho_I(\mathbf{r})}+\frac{\delta F^e}{\delta\rho_I(\mathbf{r})}, \tag{5}$$

$$=-U_I(\mathbf{r})+\mu_I^c(\mathbf{r})+\mu_I^e(\mathbf{r}). \tag{6}$$

Here we have introduced the cohesive potential μ_I^c and the excluded volume potential μ_I^e. For the cohesive interactions we employ a two-body mean-field potential

$$F^c[\rho]=\frac{1}{2}\sum_{IJ}\ \int\int\epsilon_{IJ}(|\mathbf{r}-\mathbf{r}'|)\rho_I(\mathbf{r})\rho_J(\mathbf{r}')d\mathbf{r}\ d\mathbf{r}', \tag{7}$$

$$\mu_I^c(\mathbf{r})\equiv\frac{\delta F^c}{\delta\rho_I}=\sum_J\ \int_V\epsilon_{IJ}(|\mathbf{r}-\mathbf{r}'|)\rho_J(\mathbf{r}')d\mathbf{r}', \tag{8}$$

where $\epsilon_{IJ}(|\mathbf{r}-\mathbf{r}'|)=\epsilon_{JI}(|\mathbf{r}-\mathbf{r}'|)$ is a cohesive interaction between beads of type I at $\mathbf{r}$ and J at $\mathbf{r}'$, defined by the same Gaussian kernel as in the ideal Gaussian chain Hamiltonian

$$\epsilon_{IJ}(|\mathbf{r}-\mathbf{r}'|)\equiv\epsilon^0_{IJ}\left(\frac{3}{2\pi a^2}\right)^{3/2}e^{-3/(2a^2)(\mathbf{r}-\mathbf{r}')^2}. \tag{9}$$

Existing (compressibility) models that account for excluded volume interactions will be discussed in the next sections. In equilibrium $\mu_I(\mathbf{r})$ is constant; this yields the familiar self-consistent field equations for Gaussian chains, given a proper

choice for F^{nid}. When the system is not in equilibrium the gradient of the intrinsic chemical potential $-\nabla\mu_I$ acts as a thermodynamic force which drives collective relaxation processes. When the Onsager coefficients are constant the stochastic diffusion equations are of the following form:

$$\frac{\partial\rho_I}{\partial t}=-\nabla\cdot\mathbf{J}_I, \tag{10}$$

$$\mathbf{J}_I=-M\nabla\mu_I+\tilde{\mathbf{J}}_I, \tag{11}$$

where M is a mobility coefficient and $\tilde{\mathbf{J}}_I$ is a noise field, distributed according to a fluctuation-dissipation theorem [8]. Nonlocal forms for the Onsager coefficients will be discussed in a future publication.

B. Incompressible systems

In [1], we discussed *incompressible* systems. In this special limit there is an additional dynamic constraint which conserves the total space packing in every point in space at all times [40]

$$\sum_I \nu_I\mathbf{J}_I=\mathbf{0}. \tag{12}$$

Here, ν_I is the molecular volume of bead I. Now the intrinsic chemical potential is given by $\mu_I=-U_I+\mu_I^c+\lambda$, where the Lagrange multiplier field λ replaces μ_I^e. Combining Eqs. (10) and (12), and leaving out the noise, we obtain

$$\nabla\lambda=-\frac{1}{\Sigma_I\nu_I}\sum_I \nu_I\nabla[-U_I+\mu_I^c].$$

Reinsertion of the expression for $\nabla\lambda$ in Eq. (10), shows that the dynamics is governed by exchange thermodynamic forces only. In a binary mixture the forces are of the form

$$-\nabla(\mu_A-\mu_B)=-\nabla(-U_A+U_B+\mu_A^c-\mu_B^c).$$

The cohesive interaction parameters enter the dynamic equations through the exchange parameter χ

$$\chi\equiv\frac{\beta}{2}[\nu_B^{-1}\epsilon_{AB}^0+\nu_A^{-1}\epsilon_{BA}^0-\nu_A^{-1}\epsilon_{AA}^0-\nu_B^{-1}\epsilon_{BB}^0]. \tag{13}$$

It must be realized, that in this limit the effective contribution from excluded volume interactions is a purely mathematical artifice. The constraining field λ is obtained from a dynamic constraint, and not from an underlying microscopic interaction model.

C. A simple cell model

We make the following simplifying assumptions: (i) cohesive and excluded volume interactions are local and independent and (ii) do not depend on chain length. Assumption (i) is the standard van der Waals approximation. The assumptions are (very) crude in the light of modern molecular theory [29], but we believe that for engineering purposes they are sufficient. The derivation of the free energy is straightforward. There is, however, a subtle effect which deserves special attention. In our free energy functional for the Gaussian chains there is already an ideal gas contribution included, via the partition functional for the ideal chains in the external field. In the van der Waals approximation we use here, the excluded volume effect can be cast in a correction factor C, such that $Q_{\mathrm{liquid}}=CQ_{\mathrm{gas}}$, where Q is the number of accessible states in an ideal liquid (Q_{liquid}) and the ideal gaseous state (Q_{gas}), respectively. Hence, the free energy for the excluded volume interactions is the excess free energy of the liquid over the gas, with $\beta F^e=-\ln C=-m\ln c$, where m is the total number of beads and c is the correction factor or insertion probability for each bead separately. Here, we have made explicit use of assumption (ii). Extending this definition to inhomogeneous liquids, and assuming that the insertion probability does not depend on concentration gradients (making a first-order approximation), we find the free energy functional

$$\beta F^e[\rho]=-\sum_I\int_V\rho_I(\mathbf{r})\ln c(\mathbf{r})d\mathbf{r}. \tag{14}$$

The insertion probability is interpreted as the *effective* fraction of free space. The lower the fraction of free space, the lower the insertion probability and the higher the excess free energy. In principle we could use here any of the excess free energy functions that have been proposed for liquids [29]. As we argued in the Introduction, the (modified) cell model (of the van der Waals type) is most widely used in polymer applications, it is not computationally demanding and of reasonable accuracy. The simple Carnahan-Starling equation is based on an integral equation approach and of very high accuracy in the entire phase diagram. Therefore, we only consider the following three simple models here:

$$c=\begin{cases}1-f & \text{van der Waals}\\ (1-f^{1/3})^3 & \text{cell model}\\ e^{-[f(4-3f)]/(1-f)^2} & \text{Carnahan-Starling.}\end{cases}$$

The corresponding excluded volume potentials are

$$\beta\mu_I^e\equiv\beta\frac{\delta F^e}{\delta\rho_I}$$
$$=\begin{cases}-\ln(1-f)+\dfrac{f_I}{1-f} & \text{van der Waals}\\ -\ln(1-f^{1/3})^3+\dfrac{f_I}{f^{2/3}-f} & \text{cell model}\\ \dfrac{f(4-3f)}{(1-f)^2}+f_I\dfrac{2(2-f)}{(1-f)^3} & \text{Carnahan-Starling.}\end{cases} \tag{15}$$

The concentration variables are defined by

$$\theta_I\equiv\nu_I\rho_I,$$

$$f\equiv\sum_I\theta_I,$$

$$f_I\equiv\nu_I\sum_J\rho_J=\sum_J\frac{\nu_I}{\nu_J}\theta_J.$$

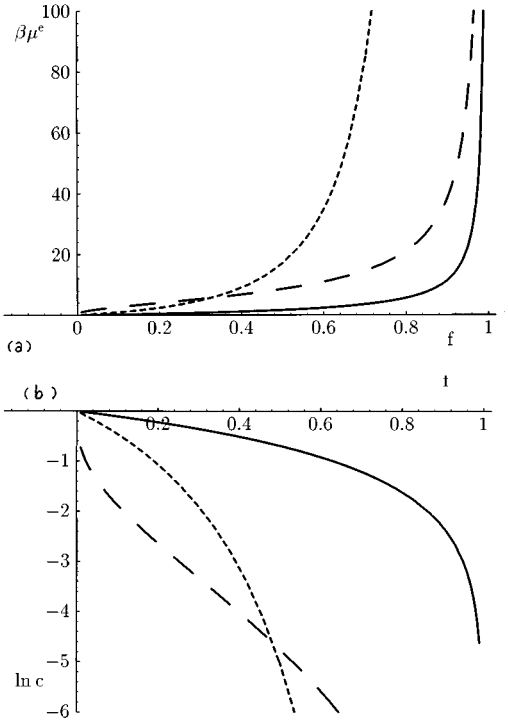

FIG. 1. (a) $\beta\mu_I^e$ as a function of the packing fraction f with $\nu_I=\nu$ for the van der Waals model (—), the cell model (— — —), and the Carnahan-Starling model (– – – – –). (b) $\ln c$ as a function of the packing fraction f with $\nu_I=\nu$ for the van der Waals model (—), the cell model (— — —), and the Carnahan-Starling model (– – – – –).

Here θ_I is a relative concentration and f is the total packing fraction. There are a two interesting limiting behaviors.

(i) In Figs. 1(a) and 1(b) we plotted $\beta\mu_I^e$ and the insertion probability c against f for the three packing models. We have set $\nu_I=\nu$. Near $f=1\beta\mu_I^e$ diverges, and the insertion probability drops to zero ($\ln c\rightarrow-\infty$), because it is impossible to fill space over 100%. In the range of typical values of f in liquid mixtures ($f\approx 0.4$–0.7), μ_I^c is about 10–30 kT, and the insertion probability is already very small (in the cell model and Carnahan-Starling model). The excluded volume effect is thus very *strong*, in fact about as strong as the opposing cohesive energy interactions [33].

From Fig. 1(b) it follows that the packing penalty in the van der Waals model is much too low, while in the liquid range the cell model behaves similarly to the Carnahan-Starling model. The best choice for the excluded volume potential in hard sphere liquids is the Carnahan-Starling equation [29], but we believe that for polymer liquids this choice gives a false impression of accuracy. We must remember that in the Gaussian spring model a single bead, or statistical unit, represents a fluctuating string of monomers, and these strings probably have a lower packing penalty than individual hard spheres. We will therefore concentrate on the cell model in the *dynamics* simulations.

(ii) In a homogeneous equilibrium system the external potential U is zero by definition, therefore $\Phi[U=0]=\Phi_0=V/\Lambda^3$, $\rho_I[U=0]=\rho_{0I}=nN_I/V$ and the free energy functional is given by

$$\beta F[U=0]=\beta F_0=-n\,\ln\frac{V}{\Lambda^3}+\ln n!-nN\,\ln c_0+\frac{1}{2}\,\beta\sum_{IJ}\,\epsilon_{IJ}^0 nN_I\rho_{0J}\,. \tag{16}$$

The equation of state is given by

$$p_0\equiv-\left(\frac{\partial F_0}{\partial V}\right)_T=p_0^{\rm id}+p_0^e+p_0^c\,, \tag{17}$$

with separate contributions from the entropy of the ideal gas of chain molecules $\beta p_0^{\rm id}=n/V$, the cohesive interactions $p_0^c=\frac{1}{2}\Sigma_{IJ}\epsilon_{IJ}^0\rho_{0I}\rho_{0J}$, and the excluded volume interactions. For the cell model we have

$$\beta p_0^e=\frac{f_0^{1/3}}{(1-f_0^{1/3})}\,\sum_I\,\rho_{0I}\,.$$

Thus the pressure of the homogeneous system does not depend on the sequence of the beads. If we set $\nu_I=\nu$, as above, then $f_0=\nu\Sigma_I\rho_{0I}=\nu nN/V$ and the equation of state simplifies to

$$\nu\beta p_0=\frac{1}{N}\,f_0+\frac{f_0^{4/3}}{(1-f_0^{1/3})}+\nu\beta p_0^c\,.$$

This equation of state is almost identical to the equation obtained from the FOV model [12]

$$\nu\beta p_{\rm FOV}=\frac{f_0}{(1-f_0^{1/3})}+\nu\beta p_0^c\,.$$

The difference with the FOV model can be explained as follows. By definition, the excluded volume free energy is an excess free energy. Since in our approach we take the excess of ideal chain liquid over ideal chain gas, the equation of state correctly reduces to the ideal gas equation for low concentration of chains, $\beta p=n/V$. In the FOV model the excess is erroneously taken with respect to a gas of free beads, and for low concentration of chains $\beta p=nN/V$. This is the ideal gas law for a system in which all beads would be *disconnected*, which is of course not correct. For practical purposes the difference between the two models is small however; in the ideal case ($\epsilon_{IJ}^0=0$) the maximal relative difference of $(p_0/p_{\rm FOV}-1)=f_0^{1/3}-1$ is found for $N=\infty$. This amounts to ca. 16% for a typical liquid packing fraction of $f_0=0.6$.

For comparison we have plotted the pressure of the homogeneous liquid according to the van der Waals model, cell model, FOV model, and Carnahan-Starling model in Fig. 2, using $\nu_I=\nu$, $N\rightarrow\infty$ and $\epsilon_{IJ}^0=0$

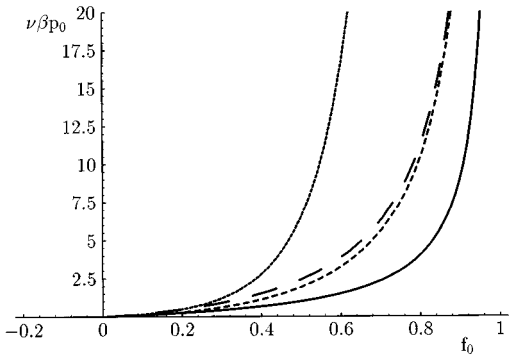

FIG. 2. $\nu\beta p_0$ as a function of f_0 for the van der Waals model (—), the Flory-Orwoll-Vrij model (— — —), the cell model (– – – – –), and the Carnahan-Starling model (– – – – – – – –).

$$\nu\beta p_0 = \begin{cases} \dfrac{f_0}{(1-f_0)} & \text{van der Waals} \\ \dfrac{f_0}{(1-f_0^{1/3})} & \text{Flory-Orwoll-Vrij} \\ \dfrac{f_0^{4/3}}{(1-f_0^{1/3})} & \text{cell model} \\ \dfrac{f_0(1+f_0+f_0^2-f_0^3)}{(1-f_0)^3} & \text{Carnahan-Starling.} \end{cases}$$

As can be concluded from Fig. 2 the FOV model and the cell model differ little, while the Carnahan-Starling model predicts a substantial larger pressure. We argued already that the Carnahan-Starling model is probably not applicable to polymer liquids.

D. Helfand's penalty function

The application of the cell model in the current algorithms for the dynamics simulation leads to a special problem. Each system possesses an optimum equilibrium space packing in which it will try to settle locally during the simulations. Due to the conservative set of equations, the total amount of material is preserved. Since the volume is constant, the mesoscopic dynamics model simulates an nVT ensemble, in which the pressure varies. Hence, if the initial volume fraction is chosen too low the system develops a liquid-gas phase transition, with gas bubbles and condensed phases dispersed throughout the system (Fig. 8). In an npT ensemble, the system volume will adjust to compensate for changes in pressure.

We could add a pressure coupling to the dynamics algorithms, similar to the pressure coupling algorithms developed for molecular dynamics simulations, but this will increase the complexity of the algorithms and will be postponed to a future publication. Here, we consider as an alternative a very simple but practical solution, which resolves the problem albeit at the cost of further approximations. The idea is originally from Helfand [36]. The ansatz is that in a liquid mixture the density fluctuations are small and harmonic, so that for the purpose of calculating phase separation the bare cohesive energy interactions ϵ_{IJ} may effectively be replaced by exchange interactions $\Delta\epsilon_{IJ}$ (with $\Delta\epsilon_{II}=0$ and $\Delta\epsilon_{IJ\neq I}\geqslant 0$). The Helfand free energy is similar to

$$F^{\mathrm{nid}}[\rho]=F^{c,\mathrm{ex}}[\rho]+\frac{\kappa_H}{2}\int\left(\sum_I \nu_I\rho_I-\sum_I \nu_I\rho_{0I}\right)^2 d\mathbf{r}, \tag{18}$$

where κ_H is a compressibility parameter. $F^{c,\mathrm{ex}}$ is the free energy resulting from the cohesive interactions, which now contains the exchange parameters only. The intrinsic chemical potential is now given by

$$\mu_I(\mathbf{r})=-U_I(\mathbf{r})+\sum_J \int_V \Delta\epsilon_{IJ}(|\mathbf{r}-\mathbf{r}'|)\rho_J(\mathbf{r}')d\mathbf{r}'$$

$$+\kappa_H\nu_I\sum_J \nu_J\rho_J(\mathbf{r}), \tag{19}$$

where we have omitted an unimportant constant term $\Sigma_J\nu_J\rho_{0J}$. In general, a penalty function will allow small density fluctuations around the mean bulk density. In this approach, κ_H is a global constant, independent of composition, that can be related to experimental values of isothermal compressibility [37]. If the compressibility of the pure components is very different, effective composition dependent κ_H have to be introduced.

III. COMPARISON OF DYNAMIC BEHAVIOR

A. Analytical results

The three dynamic models for the excluded volume effects (incompressible, cell model, and Helfand penalty) each involve the integration of highly coupled nonlinear equations. It is therefore not easy to see how the various approximations affect the dynamic behavior. However, it is illustrative to compare the consequences of the three models for the stability of the packing fraction field f. Suppose that in the block copolymer melt the molecular volumes of the two species are the same. We replace the interaction kernels $\epsilon_{IJ}(|\mathbf{r}-\mathbf{r}'|)$ by δ functions $\epsilon_{IJ}^0\delta(\mathbf{r}-\mathbf{r}')$ (local interactions only). Furthermore, we assume that the cohesive energy parameters for the individual components are also the same, with $\beta\epsilon_{AA}^0\nu^{-1}=\beta\epsilon_{BB}^0\nu^{-1}=\epsilon$, and a weak difference between A and B $\beta\epsilon_{AB}^0\nu^{-1}=\beta\epsilon_{BA}^0\nu^{-1}=\epsilon+\chi$. Typically, ϵ is between -10 and -50, while $\chi\approx O(1)$. We define the local order parameter by

$$\pi\equiv\theta_A-\theta_B.$$

The dynamics equations (10) for each of the two components A and B can be rewritten to a dynamics equation for π and a dynamics equation for f. In Fourier space the equations are as follows (neglecting the noise in order to simplify the analysis):

$$\frac{\partial\pi_q}{\partial t}=-Dq^2[\Delta U_q-\chi\pi_q],$$

$$\frac{\partial f_q}{\partial t}=\begin{cases} 0 & \text{incompressible} \\ -Dq^2\left[\sum U_q+(2\kappa_H'+\chi)f_q\right] & \text{penalty} \\ -Dq^2\left[\sum U_q+\sum \mu_q^c+\sum \mu_q^e\right] & \text{cell model.} \end{cases}$$

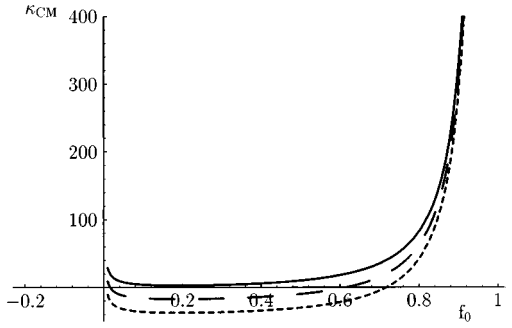

FIG. 3. κ_{CM} as a function of f_0 for $\epsilon=-10$ (—), $\epsilon=-30$ (— — —), and $\epsilon=-50$ (– – – – –).

with $D=M\nu/\beta$, $\Delta U_q=-\beta(U_{Aq}-U_{Bq})$, $\Sigma U_q=-\beta(U_{Aq}+U_{Bq})$, $\Sigma\mu_q^i=\beta(\mu_{Aq}^i+\mu_{Bq}^i)$, and $\kappa_H'=\beta\nu\kappa_H$. In all three models, the driving force for microphase separation is generated by $\Delta U-\chi\pi_q$. In Helfand's penalty model the packing fraction f may change, depending on the parameters. In a typical situation $\Sigma U\approx O(1/N)$, so that the penalty function in the evolution equation for f dominates, provided $\kappa_H'\gg 1$. In this case the total packing fraction has an ideal diffusive behavior

$$\left(\frac{\partial f_q}{\partial t}\right)_{\text{Penalty}}\approx -q^2 2\kappa_H' D f_q$$

and hence *any* inhomogeneity in the total packing fraction, whether negative or positive, will diffuse rapidly back to homogenous packing state with diffusion constant $2\kappa_H'D$.

In the cell model this is slightly more complicated. The time evolution for the order parameter in the cell model is the same as in the penalty and incompressible models. However, in this case packing inhomogeneities can arise spontaneously, as we already remarked earlier. For small deviations from homogeneity we can approximate

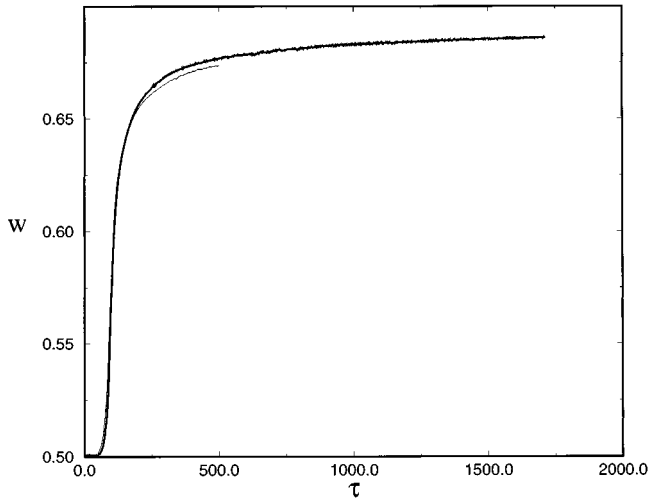

FIG. 4. Time evolution of volume-averaged order parameter w as a function of τ in an A_8B_8 block copolymer melt for the incompressible model (—) and the Helfand penalty model with $\kappa_H'=10$ (⁓). The quench from $\chi=0$ to $\chi=1$ is at $\tau=50$.

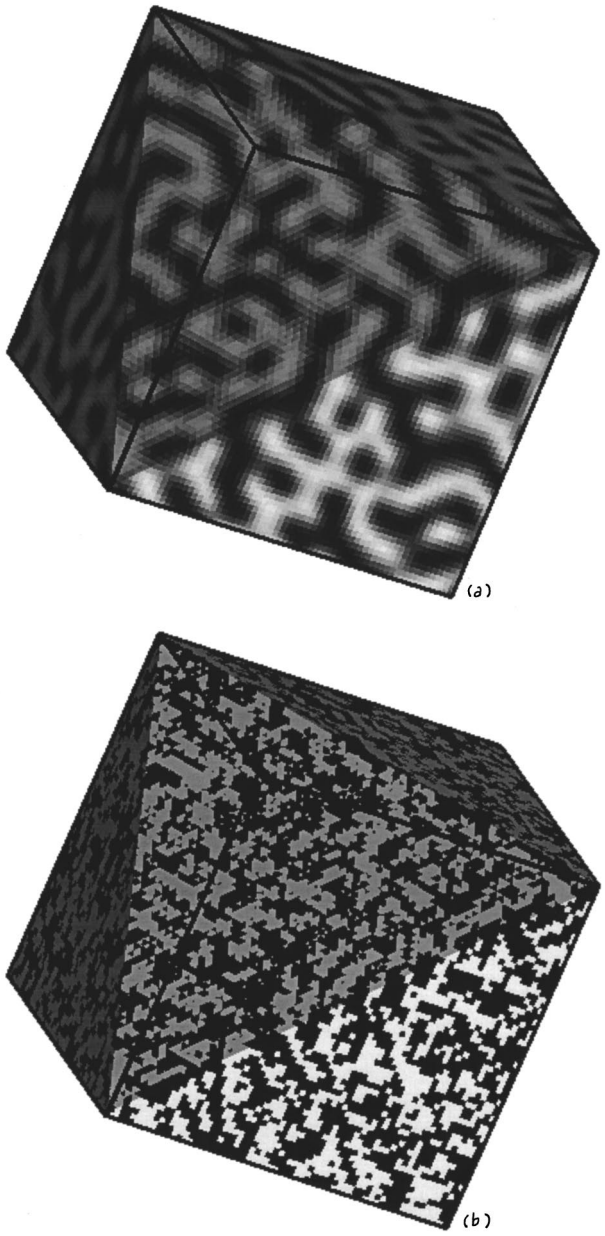

FIG. 5. Morphology of an A_8B_8 block copolymer melt at $\tau=1500$ according to the penalty model with $\kappa_H'=10$. The melt was quenched at $\tau=50$ from $\chi=0$ to $\chi=1$. (a) π, values range from -0.94–0.94 (black to white). (b) f, values range from 0.96–1.04 (black to white).

$$\sum\mu_q^e+\sum\mu_q^c=(2\kappa_{\mathrm{CM}}+\chi)f_q,$$

$$\kappa_{\mathrm{CM}}=\epsilon+\frac{4-3f_0^{1/3}}{3(-1+f_0^{1/3})^2 f_0^{2/3}}. \tag{20}$$

In Fig. 3 κ_{CM} is plotted against f_0, for various values of the cohesive interaction parameter ϵ. Clearly, if the initial packing fraction is low and/or the cohesive energy parameter is strongly negative, κ_{CM} is *negative* and this implies that an inhomogeneity in the total packing fraction will grow spontaneously (depending on the precise value for $\Sigma U_q\sim 1/N$): the system then develops regions with low and high con-

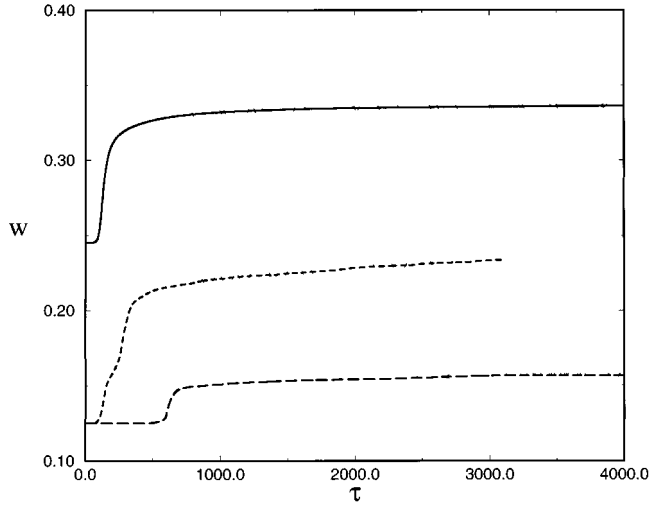

FIG. 6. Time evolution of volume-averaged order parameter w as a function of τ in an A_8B_8 block copolymer melt for the cell model at different volume fractions. (A) $f=0.7$ (—) quenched at $\tau=50$, (B) $f=0.5$ (– – – – –) quenched at $\tau=50$, and (C) $f=0.5$ (— — —) not quenched.

densed phases. If κ_{CM} is weakly positive a phase transition is still possible, leading to nucleation phenomena in the binodal regime [see, e.g., Fig. 8(a)]. If we select the conditions such that $\kappa_{\mathrm{CM}} \gg 1$ the cell model reduces to a penalty model with non constant but positive penalty coefficient.

Notice that in the above analysis we have assumed an nVT ensemble, and thus the pressure is allowed to vary. When the pressure is kept constant, the microphase separation dynamics in the cell model can be considerably different from the penalty or incompressible model. A precise analysis of the stability conditions in the cell model including pressure effects is quite involved and will be postponed to a future publication.

B. Numerical results

We performed a number of numerical simulations, using the various excluded volume interaction models. To make a comparison with previous simulation results [1], we have used the same linear mobility coefficient [which differs from the approximation in Eq. (10)] $\mathbf{J}_I=-M\rho_I\nabla\mu_I+\tilde{\mathbf{J}}_I$, and studied the microphase separation dynamics in an A_8B_8 copolymer melt. The initial system is always homogeneous. Numerically, after discretizing the dynamic equations on a grid [cf. Eq. (10)], we have the following Crank-Nicolson equations for each component I

$$\theta_{Ir}^{k+1}-\omega\Delta\tau z_{Ir}^{k+1}=\theta_{Ir}^{k}+(1-\omega)\Delta\tau z_{Ir}^{k}+\eta_{Ir}^{k}.$$

Here, η_{Ir}^{k} is the noise which is distributed according to a fluctuation-dissipation theorem [8]. Notice that the noise is applied at every time step. z_r^k denotes the discretized diffusion part at time level k and (cubic) grid position r

$$z_r=\sum_{\alpha}\sum_{q} d_{\alpha}[D_{\alpha}\theta_I D_{\alpha}]_{rq}\beta\mu_{Iq}.$$

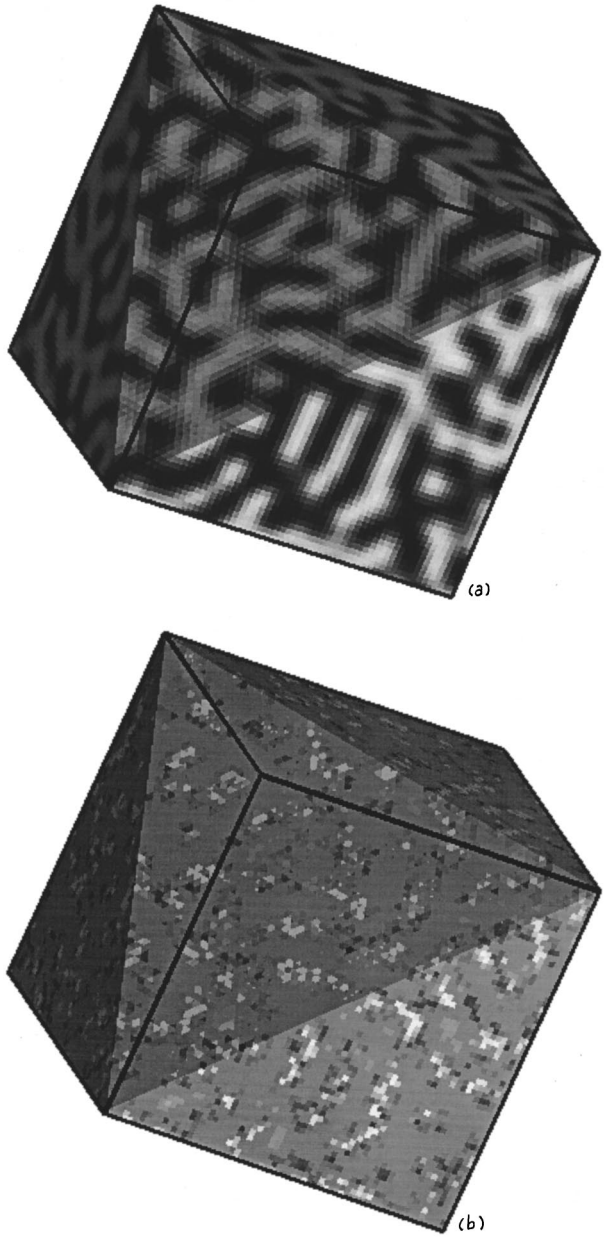

FIG. 7. [Illustration of simulation (A)]. Morphology of an A_8B_8 copolymer melt at $\tau=1500$ according to the cell model. The interaction parameters are explained in the text. The melt was quenched at $\tau=50$ from $\chi=0$ to $\chi=1$. (a) π, values range from -0.65–0.69 (black to white). (b) f, values range from 0.66–0.76 (black to white).

D_{α} is the discretized diffusion operator in grid direction α and μ_{Iq} is evaluated at grid position q. ω is the Crank-Nicolson parameter and $\Delta\tau$ is a scaled time step. The Crank-Nicolson equations are solved iteratively at every time step using a steepest descent method. We define an average measure of the order in the system by

$$w\equiv\frac{1}{V}\int_V(\theta_A^2+\theta_B^2)d\mathbf{r}=\frac{1}{2V}\int_V(f^2+\pi^2)dr.$$

w captures the effects of a change in order due to microphase separation and/or total density fluctuations. In Fig. 4 we plot-

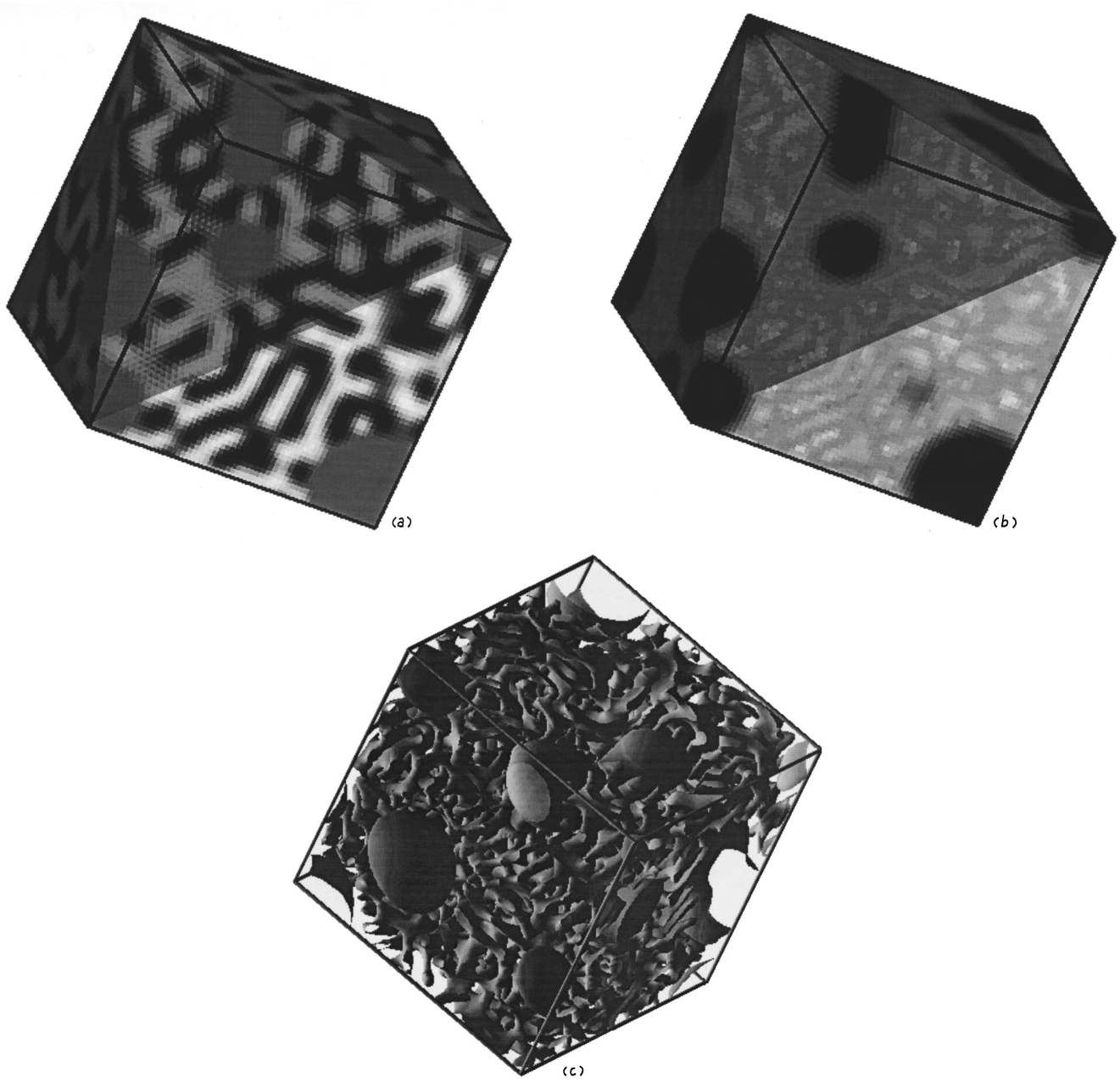

FIG. 8. [Illustration of simulation (B)]. Morphology of an A_8B_8 copolymer melt at $\tau=1500$ according to the cell model. Interaction parameters are explained in the text. The melt was quenched at $\tau=50$ from $\chi=0$ to $\chi=1$. (a) π, values range from -0.62–0.62 (black to white). (b) f, values range from 0.0–0.66 (black to white). (c) Isosurface representation of $U_A+U_B=0$, values range from -0.61–1.54.

ted the time evolution of w in a simulation using the incompressible model (all parameters as in [1]) and Helfand's penalty model ($\kappa_H'=10$). The phase separation was initiated with a quench from $\chi=0$ to $\chi=1.0$ at $\tau=50$. Figure 4 clearly shows that the models have the same dynamic performance (the penalty model was followed over a longer period of time for stability tests). Notice that in the incompressible model, the numerical errors effectively allow density fluctuations of the same order as in the penalty model. In the interfacial regions the packing fraction has a dip of a few percent [illustrated in Figs. 5(a) and 5(b)], which was absent in the incompressible model simulations. The depth of the dip strongly depends on the compressibility parameter; the larger κ_H, the smaller the dip.

More interesting effects are observed in simulations using the cell model. In Fig. 6 the time evolution of the average order parameter is plotted for three different simulations. In the three cases $\beta\epsilon_{IJ}^0\nu^{-1}=-20.0$ initially, in simulations A and B the interactions are quenched to $\beta\epsilon_{AB}^0\nu^{-1}=\beta\epsilon_{BA}^0\nu^{-1}=-18.57$ and $\beta\epsilon_{AB}^0\nu^{-1}=\beta\epsilon_{BA}^0\nu^{-1}=-18.0$, respectively, at $\tau=50$. The initial volume fractions are $f_0=0.7$ (A) and $f_0=0.5$ (B and C). The quenched interaction values correspond to $\chi\theta_{0B}=0.5$ effectively, as in the incompressible system. In simulation C the system is *not* quenched.

Figure 6 clearly shows a fast increase of the order parameter after the quench at $\tau=50$ for simulations A and B; a sign of microphase separation. In case B the order parameter

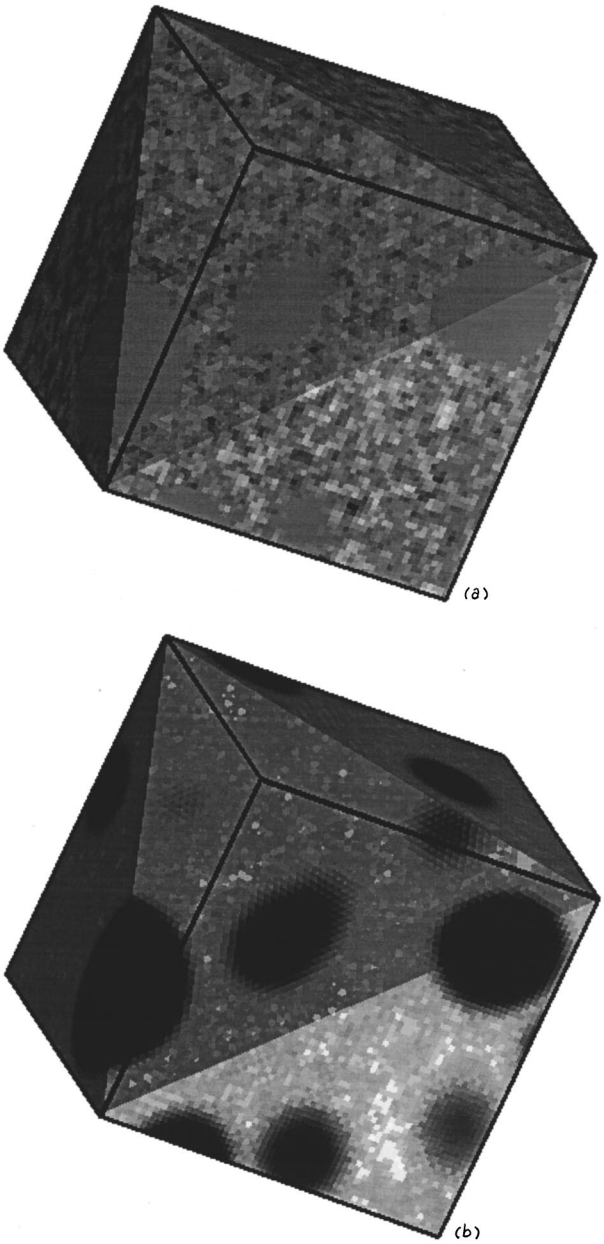

FIG. 9. [Illustration of simulation (C)]. Morphology of an A_8B_8 copolymer melt at $\tau=1500$ according to the cell model. Interaction parameters are explained in the text. The melt was not quenched, the excluded volume effects cause gas bubble nucleation. (a) π, values range from -0.06–0.06 (black to white). (b) f, values range from 0.0–0.65 (black to white).

does not increase smoothly; the inflection points correspond to gas bubble nucleation. The increase of the order parameter in case C is not due to microphase separation, but is a result of gas bubble development in the binodal regime ($\kappa_{CM}=0.13$ [see Eq. (20)] in both simulations B and C), due to the excluded volume effects at low packing fraction.

Figures 7(a)–9(a) are illustrations of the different morphologies at $\tau=1500$ for the three simulations. Because the system can not adapt its volume to pressure changes, gas bubbles develop if the initial packing fraction is too low [Figs. 8(a) and 9(a)]. Figures 7(b) and 8(b) show the packing

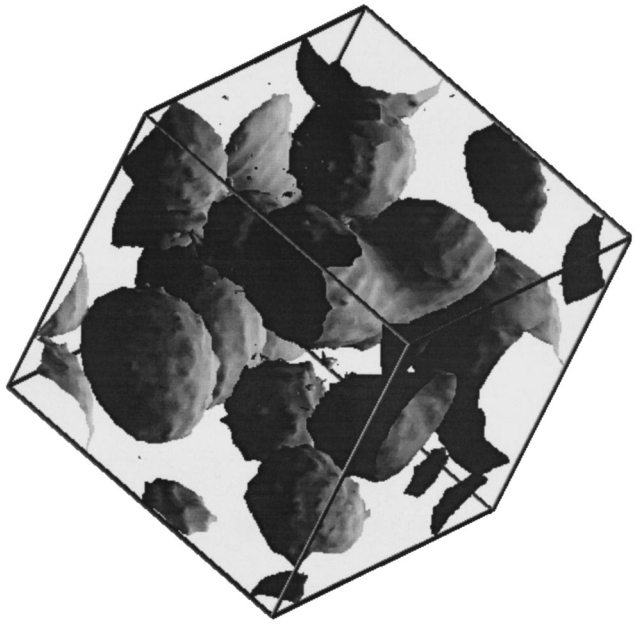

FIG. 10. Isosurface representation of $f=0.6$ at $\tau=1500$ in simulation B. (See Fig. 8 for parameters.) The gas bubbles are clearly visible.

fraction at $\tau=1500$ for the two simulations. In comparing figures (a) and (b) we see that the black regions in 7(b) and 8(b) indicate density dips at domain interfaces. The interface effects are much less in the cell model simulations than in the penalty model simulations. Notice that the effective $\kappa_{CM}=25.0$ and is, hence, much higher in the cell model simulations than in the penalty model simulations. The maximum packing fraction is increased with respect to the initial packing fraction in simulations B and C because of the nucleation phenomena.

From Figs. 8(a), 8(c), and 10 we conclude that the microphase separated domains have an orientation *towards* the gas-liquid interface, rather than an adjacent or parallel orientation. We will further investigate this orientation in future simulations.

IV. CONCLUSION

In this paper we have examined the effects of different compressibility models on numerical simulations of copolymer melts using the dynamic mean-field density functional method. Our results clearly show that a cell model (a modification of the FOV model) can be used, which exhibits physical excluded volume effects (density dips at domain interfaces). The usage of the cell model also causes gas bubble nucleation at low initial packing fractions in nVT simulations. This effect will not be present in npT simulations, where the system will adapt its volume to pressure changes. The resulting morphologies show intriguing structures, with lamellar phases oriented towards the gas-liquid interface. The interface effects are even more clear if the phenomenological penalty model is used, which is mathematically and numerically very simple and shows no gas-liquid transitions.

[1] J. G. E. M. Fraaije, B. A. C. Van Vlimmeren, N. M. Maurits, M. Postma, O. A. Evers, C. Hoffmann, P. Altevogt, and G. Goldbeck-Wood, J. Chem. Phys. **106**, 4260 (1997).
[2] M. C. Cross and P. C. Hohenberg, Rev. Mod. Phys. **65**, 851 (1993).
[3] P. C. Hohenberg and B. I. Halperin, Rev. Mod. Phys. **49**, 435 (1977).
[4] O. T. Valls and J. E. Farrell, Phys. Rev. E **47**, R36 (1993).
[5] T. Kawakatsu, K. Kawasaki, M. Furusaka, H. Okabayashi, and T. Kanaya, J. Chem. Phys. **99**, 8200 (1993).
[6] A. Shinozaki and Y. Oono, Phys. Rev. E **48**, 2622 (1993).
[7] B. Schmittmann and R. K. P. Zia, in *Phase Transitions and Critical Phenomena*, edited by C. Domb and J. Lebowitz (Academic, London, 1994).
[8] B. A. C. Van Vlimmeren and J. G. E. M. Fraaije, Comput. Phys. Commun. **99**, 21 (1996).
[9] N. M. Maurits, P. Altevogt, O. A. Evers, and J. G. E. M. Fraaije, Comp. Polym. Sci. **6**, 1 (1996).
[10] N. M. Maurits and J. G. E. M. Fraaije, J. Chem. Phys. **106**, 6730 (1997).
[11] B. A. C. Van Vlimmeren, M. Postma, P. Huetz, A. Brisson, and J. G. E. M. Fraaije, Phys. Rev. E **54**, 5836 (1996).
[12] P. J. Flory, R. A. Orwoll, and A. Vrij, J. Am. Chem. Soc. **86**, 3507 (1964).
[13] A. T. DiBenedetto, J. Polym. Sci. Part A **1**, 3459 (1963).
[14] V. S. Nanda and R. Simha, J. Phys. Chem. **68**, 3158 (1964).
[15] V. S. Nanda, R. Simha, and T. Somcynsky, J. Polym. Sci. Part C **12**, 277 (1966).
[16] R. Simha and T. Somcynsky, Macromolecules **2**, 342 (1969).
[17] B. Hartmann and M. A. Hague, J. Appl. Polym. Sci. **30**, 1553 (1985).
[18] B. Hartmann and M. A. Hague, J. Appl. Phys. **58**, 2831 (1985).
[19] I. C. Sanchez and R. H. Lacombe, J. Phys. Chem. **80**, 2352 (1976).
[20] I. C. Sanchez and A. C. Balazs, Macromolecules **22**, 2325 (1989).
[21] C. G. Panayiotou, Macromolecules **20**, 861 (1987).
[22] P. Zoller, J. Polym. Sci. Polym. Phys. Ed. **18**, 157 (1980).
[23] G. T. Dee and D. J. Walsh, Macromolecules **21**, 811 (1988).
[24] R. Dickman and C. K. Hall, J. Chem. Phys. **85**, 4108 (1986).
[25] P. J. Flory, R. A. Orwoll, and A. Vrij, J. Am. Chem. Soc. **86**, 3515 (1964).
[26] P. J. Flory, J. Am. Chem. Soc. **87**, 1833 (1965).
[27] B. E. Eichinger and P. J. Flory, Trans. Faraday Soc. **64**, 2035 (1968).
[28] S. Janssen, D. Schwahn, K. Mortensen, and T. Springer, Macromolecules **26**, 5587 (1993).
[29] Jean Pierre Hansen and Ian R. McDonald, *Theory of Simple Liquids* (Academic, London, 1986).
[30] K. S. Schweizer and J. G. Curro, Phys. Rev. Lett. **60**, 809 (1988).
[31] K. G. Honnell, J. G. Curro, and K. S. Schweizer, Macromolecules **23**, 3496 (1990).
[32] James P. Donley, John G. Curro, and John D. McCoy, J. Chem. Phys. **101**, 3205 (1994).
[33] D. Porter, *Group Interaction Modelling of Polymer Properties* (Dekker, New York, 1995).
[34] D. W. Krevelen, *Properties of Polymers, Their Correlation with Chemical Structure; Their Numerical Estimation and Prediction from Additive Group Contribution*, 3rd ed. (Elsevier, Amsterdam, 1990).
[35] R. S. Spencer and G. D. Gilmore, J. Appl. Phys. **20**, 502 (1949).
[36] E. Helfand, J. Chem. Phys. **62**, 999 (1975).
[37] D. T. Wu, G. H. Fredrickson, J.-P. Carton, A. Ajdari, and L. Leibler, J. Polym. Sci. Part B **33**, 2373 (1995).
[38] P. G. de Gennes, *Scaling Concepts in Polymer Physics* (Cornell University, Ithaca, 1979).
[39] M. Doi and S. F. Edwards, *The Theory of Polymer Dynamics* (Clarendon, Oxford, 1986).
[40] P. G. de Gennes, J. Chem. Phys. **72**, 4756 (1980).